Structural characterization of oxidized allotaxially grown $CoSi_2$ layers by x-ray scattering

I. D. Kaendler
Institut für Experimentelle und Angewandte Physik, Christian-Albrechts-Universität Kiel, Leibnizstrasse 17-19, 24098 Kiel, Germany and APS/XFD Argonne National Laboratory, 9700 South Cass Avenue, Argonne, Illinois 60439-4814

O. H. Seeck
APS/XFD Argonne National Laboratory, 9700 South Cass Avenue, Argonne, Illinois 60439-4814

J.-P. Schlomka, M. Tolan, W. Press, and J. Stettner
Institut für Experimentelle und Angewandte Physik, Christian-Albrechts-Universität Kiel, Leibnizstrasse 17-19, 24098 Kiel, Germany

L. Kappius
Institut für Schicht-und Ionentechnik, Forschungszentrum Jülich GmbH, 52425 Jülich, Germany

C. Dieker
Institut für Schicht-und Ionentechnik, Forschungszentrum Jülich GmbH, 52425 Jülich, Germany and Technische Fakultät Christian-Albrechts-Universität Kiel, Kaiserstrasse 2, 24143 Kiel, Germany

S. Mantl
Institut für Schicht-und Ionentechnik, Forschungszentrum Jülich GmbH, 52425 Jülich, Germany

(Received 13 May 1999; accepted for publication 21 September 1999)

A series of buried $CoSi_2$ layers prepared by a modified molecular beam epitaxy process (allotaxy) and a subsequent wet-oxidation process was investigated by x-ray scattering. The oxidation time which determines the depth in which the $CoSi_2$ layers are located within the Si substrates has been varied during the preparation. The electron density profiles and the structure of the interfaces were extracted from specular reflectivity and diffuse scattering measurements. Crystal truncation rod investigations yielded the structure on an atomic level (crystalline quality). It turns out that the roughness of the $CoSi_2$ layers increases drastically with increasing oxidation time, i.e., with increasing depth of the buried layers. Furthermore, the x-ray data reveal that the oxidation growth process is diffusion limited. © *2000 American Institute of Physics.* [S0021-8979(00)00901-4]

I. INTRODUCTION

The growth of thin metallic silicides on silicon is of great technological relevance. Silicides are used in integrated circuits as contacts and interconnections. Epitaxial $CoSi_2$ silicides can be produced by molecular beam epitaxy (MBE)[1–3] or ion beam synthesis (IBS).[4–6] Both techniques, MBE and IBS, have been successfully employed to produce high quality $CoSi_2$ layers. Many studies concentrated on the detailed structural questions concerning these growth modes. A modified MBE process (allotaxy) was developed by S Mantl *et al.* to produce epitaxial $CoSi_2$ films also on Si(001) surfaces.[7,8] The structural and interfacial properties of allotaxially grown films were studied by x-ray diffraction in a preceding work.[3] In this article, we present a systematic study of the interfacial and the atomic structure of allotaxially grown $CoSi_2$ samples which have been treated by a subsequent wet-oxidation process. Oxidation produces a SiO_2 layer on top of the silicide layer which is pushed deeper into the substrate without loosing its integrity. Recently it has been shown that local oxidation of thin epitaxial $CoSi_2$ films is a new versatile method for producing silicide nanostructures.[9–13]

For applications in microelectronic devices the interfacial roughness and the homogeneity of the layer systems is of great importance. Since the oxidation process may alter these properties drastically, a study of samples in different stages of oxidation was necessary. In this work, we have studied the mesoscopic properties (e.g., film thicknesses and roughnesses) and the atomic structure (i.e., the crystalline quality and lattice parameters) of various samples grown by molecular beam allotaxy (MBA). X-ray reflectivity was used to monitor the vertical density profile and diffuse scattering for the investigation of the lateral interface structure. Additionally, crystal truncation rods (CTRs) in the vicinity of Bragg reflections were measured to obtain information about the atomic structure (crystalline quality). Furthermore, transmission electron microscopy (TEM) was applied to compare the x-ray results which yield a global averaged picture of the samples, with the local information from the TEM images.

This article is organized as follows: In Sec. II the samples and the sample preparation are presented. Section III contains a description of the x-ray experiments and the data analysis. The results are discussed in terms of the preparation conditions in Sec. IV.

II. SAMPLES AND PREPARATION

Epitaxial $CoSi_2$ layers on Si(001) with thicknesses of 300 Å were grown by MBA at a substrate temperature of

TABLE I. Specifications of the six MBA $CoSi_2$ samples with subsequently grown SiO_2 cap layers. The thickness of the $CoSi_2$ layer is ~300 Å for each sample.

Sample	Oxidation time (min)	SiO_2 thickness (Å)
CS#1	0	50–100
CS#2	3	790
CS#3	7	1050
CS#4	10	1460
CS#5	15	1740
CS#6	20	1990

380 °C.[7,8] Subsequently, wet oxidation was applied to six samples to grow SiO_2 on top of the silicide layer. During MBA growth the Si deposition rate was kept constant, whereas the deposition rate of the Co was increased linearly until the peak concentration of 31% was reached. This produced small and discrete precipitates of $CoSi_2$ embedded in a homogeneous Si matrix. After this a rapid thermal annealing process was applied at 1100 °C for 20 s in a 90%/10% N_2/O_2 atmosphere. The annealing leads to precipitate coalescence and finally to a homogeneous $CoSi_2$ film. Wet oxidation in steam formed an amorphous SiO_2 layer on top of the silicide. The thickness of the SiO_2 layer depends on the oxidation time. The samples are denoted as CS#1–CS#6 in the following, with a $CoSi_2$ layer of thickness $d_{CoSi_2} \approx 300$ Å and SiO_2 layer thicknesses d_{SiO_2} within the range 100 Å $< d_{SiO_2} < 2000$ Å (see Table I).

III. X-RAY EXPERIMENTS

The experiments were performed using a two-circle diffractometer. The x-ray beam was produced by a 18 kW rotating anode (Simens XP18) with a copper target. A Ge(111) monochomator selects the wavelength of the Cu $K\alpha_1$ line ($\lambda = 1.540\,56$ Å). Slits define a beam size of 0.3×5 mm^2 at the sample position. The scattered intensity is detected by a NaI scintillation counter.

We applied different x-ray techniques to measure the interfacial properties of the samples. By analyzing the specular reflectivity of each sample a vertical density profile is obtained. Particularly, the rms-roughnesses and the layer thicknesses of the interfaces can be determined accurately with this method. However, it turns out that the diffuse scattering of all samples is rather large and has to be carefully subtracted from the reflectivity data before the analysis. The diffuse scattering also contains information about the lateral structure of the interfaces, namely the lateral correlation lengths and roughness exponents.[14–22] However, in this article the diffuse scattering will be discussed only qualitatively. While reflectivity measurements in the region of small incidence and exit angles give no information about the atomic structure of the sample, measurements in the vicinity of the (004) Bragg reflection, i.e., CTR measurements, yield information about a possible strain in the grown $CoSi_2$ layers and the crystalline quality of the films in general.[23–25]

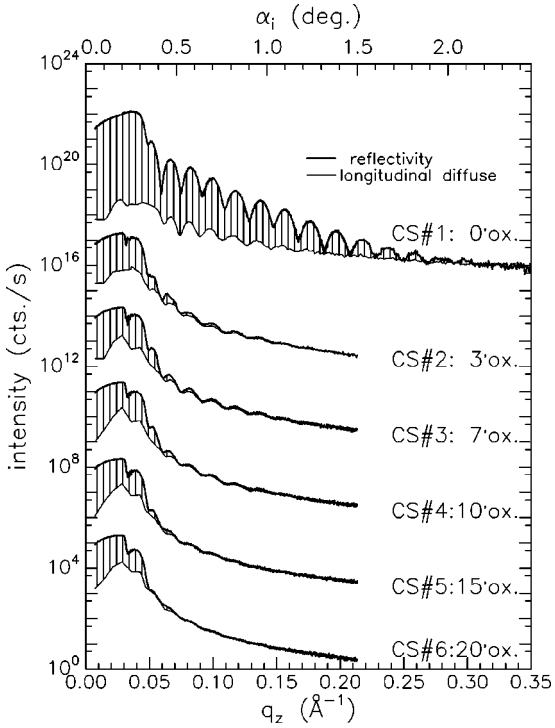

FIG. 1. Reflectivities (thick lines) and longitudinal diffuse scattering (thin lines) for the six samples CS#1–CS#6. The oxidized samples exhibit very strong diffuse scattering that dominates the reflectivities for $q_z > 0.1$ Å^{-1}. The shaded areas highlight the true specular reflectivities.

A. Specular reflectivity and diffuse scattering

The condition for specular reflectivity is $\alpha_i = \alpha_f$, i.e., the incident angle equals the exit angle during a reflectivity scan. Since the real part of the refraction index $n = 1 - \delta + i\beta$ ($\delta > 0$ dispersion, β absorption, $\delta, \beta \sim 10^{-6}$) is slightly smaller than unity for hard x rays ($\lambda \sim 1$ Å), total external x-ray reflection occurs for incident angles $\alpha_i \leqslant \alpha_c$, where $\alpha_c \simeq \sqrt{2\delta} \sim 0.2° - 0.5°$ depending on the wavelength and the material.[26] Thus, glancing angles are required. For reflectivity measurements the wave vector transfer $\mathbf{q} = \mathbf{k}_f - \mathbf{k}_i$, with the wave vectors of the incident and scattered radiation $\mathbf{k}_{i,f}$, has only a component $q_z = (4\pi/\lambda)\sin\alpha_i$ perpendicular to the sample surface. Hence x-ray reflectivity probes the vertical structure of a sample averaged over the illuminated area. The theory of specular reflectivity has been developed in the last decades and is now very well known. We have analyzed our data according to the standard procedure based on the recursive formalism given by Parratt[27] (for details, see e.g., Refs. 22, 25, and 28–31).

Figure 1 depicts the measured reflectivities of the six samples as a function of the vertical wave vector transfer q_z. Qualitatively, the following conclusions can be directly obtained from the data. All curves show a typical total external reflection plateau region for $q_z < q_{z;c,SiO_2} = 4\pi\sqrt{2\delta_{SiO_2}}/\lambda \approx 0.03$ Å^{-1}.[32] Only sample CS#1 does not show the critical q_z of SiO_2 because $CoSi_2$ forms the topmost layer. The critical q_z of $CoSi_2$ can also be seen in the data of the other samples as a feature at $q_z = q_{z;c,CoSi_2} = 4\pi\sqrt{2\delta_{CoSi_2}}/\lambda \approx 0.045$ Å^{-1}. The location of the first critical angle corresponds to the nominal bulk den-

sity of SiO_2 and the second critical angle is caused by the buried $CoSi_2$ films. This shows that for all samples the $CoSi_2$ layers and the SiO_2 films are homogeneous. For larger q_z the reflectivity drops rapidly and oscillations stemming from interference of the reflected x rays from different interfaces are superimposed over the curves. Here, the modulation period corresponds to the $CoSi_2$ layer thickness (see below). For a single layer the thickness d is related to the modulation period Δq_z via $d=2\pi/\Delta q_z$. However, the reflectivities shown in Fig. 1 *cannot* be refined directly using the Parratt algorithm because the diffuse scattering has to be subtracted carefully first.

This situation is displayed in Fig. 2, which shows four transverse scans (''rocking curves'') obtained at different fixed detector positions $\phi=\alpha_i+\alpha_f$ for sample CS#5 (see Table I). The topmost curve was measured at $\phi=0.6°$. At $\alpha_i=\phi/2$ the sharp specularly reflected peak appears on top of rather narrow diffusely scattered intensity. The intensity of the specular part is at least one order of magnitude higher than the diffuse part. This is already different for the transverse scan that has been recorded for $\phi=0.8°$ (see second curve in Fig. 2). Now only a small amount of the whole intensity at $\alpha_i=\phi/2$ corresponds to the specular reflectivity. The diffuse scattering is even larger than the reflectivity, particularly at the positions of the Yoneda peaks.[14,25,28,33] The rocking curves for $\phi=1.0°$ and $\phi=1.5°$ show that all scattering is essentially diffuse and no sharp resolution limited component can be seen. Thus, all intensity at the specular condition $\alpha_i=\phi/2$ has to be treated as diffuse scattering. The vanishing of the specular intensity at q_z values of about $q_z\sim 0.15\,\text{Å}^{-1}$ is a clear signature of rough interfaces.

The usual strategy of separating the diffuse scattering at $\alpha_i=\phi/2$ from the specular reflectivity is to perform a so-called ''longitudinal diffuse scattering scan''. This scan is basically a reflectivity with $\alpha_i+\Delta\alpha_i=\phi/2$. The offset $\Delta\alpha_i$ has to be much larger than the FWHM of the specular peak in a rocking scan. If the diffusely scattered intensities at $\alpha_i=\phi/2$ and $\alpha_i+\Delta\alpha_i=\phi/2$ are comparable, the true specular intensity is determined simply by the measured intensity at $\alpha_i=\phi/2$ minus the intensity recorded at $\alpha_i+\Delta\alpha_i=\phi/2$.

However, in our case this condition is not valid for small ϕ (see Fig. 2). For example, at $\Delta\alpha_i=0.1°$ (vertical dashed line) the diffusely scattered intensity at $\phi=0.6°$ is much lower than that at the specular condition $\Delta\alpha_i=0.0°$. At $\phi=0.8°$ the situation is reversed. We obtained the longitudinal diffuse scattering at the specular condition in the following way: (i) For very small incidence angles α_i the diffuse intensity at $\alpha_i=\phi/2$ was estimated from a few rocking scans and not by measuring a longitudinal diffuse scan. This procedure is applicable because the diffuse intensity is at least one order of magnitude less than the specular peak in this region. (ii) For large incidence angles α_i the diffuse intensity at $\alpha_i=\phi/2$ is identical to the measured diffuse intensity at an offset $\Delta\alpha_i$ except for a small intensity offset which has to be taken into account. (iii) For α_i values in the intermediate region we determined the ratios between the diffuse intensity at $\alpha_i=\phi/2$ and $\alpha_i+\Delta\alpha_i=\phi/2$ at several ϕ from some rocking scans. Depending on ϕ these ratios have been used to scale the measured longitudinal diffuse scan ($\alpha_i+\Delta\alpha_i=\phi/2$). This method is more accurate than method (i) because the measured longitudinal diffuse scan is used as the base to get the intensity at $\alpha_i=\phi/2$. After these corrections we obtain the true longitudinal diffuse intensity at the specular condition (see thin lines in Fig. 1) that has to be subtracted from the reflectivity data. Hence only the intensity marked by the shaded regions in Fig. 1 has to be taken into account for a reflectivity fit (see Fig. 3) to obtain the density profiles of the samples.

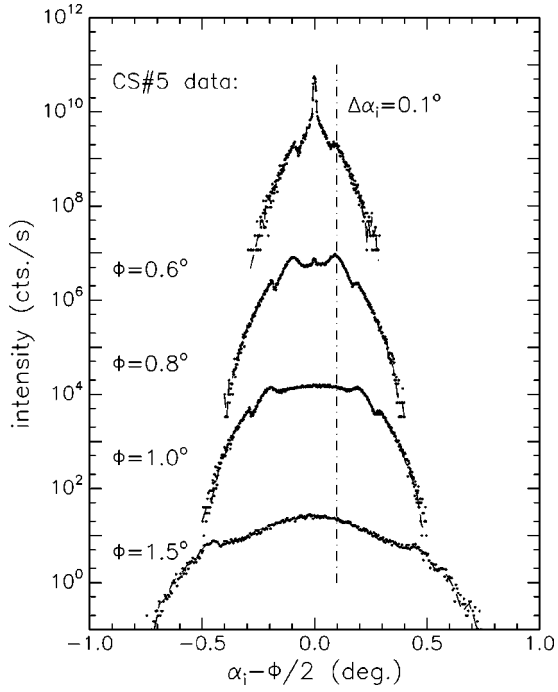

FIG. 2. Transverse (rocking) scans for sample CS#5 and different fixed detector angles $\phi=\alpha_i+\alpha_f=0.6°,\ldots,1.5°$. The dashed–dotted vertical line indicates the position of the longitudinal diffuse scans. The sharp specular peak vanishes for incidence angles $\alpha_i>0.5°$, hence the recorded intensity is purely diffuse in this region. All curves are vertically shifted for clarity.

B. Truncation rod scattering

CTRs[23–25] were measured for samples CS#1–CS#4. CTRs in the vicinity of the (004) substrate Bragg reflections were recorded by performing scans with $\alpha_i=\alpha_f$, i.e., by measuring wide angle reflectivities. The wave vector transfer $|\mathbf{q}|$ now is on the order of inverse atomic spacings. Hence, the crystalline structure is directly probed. Since $\mathbf{q}$ has again only a perpendicular component q_z, the length $2\pi/q_z$, here the spacing a of the (001) planes, is sampled.

Figure 4 depicts the CTRs of the four samples. The intense peaks at $q_z=4.627\,\text{Å}^{-1}$ are the (004) substrate Bragg reflections. The small peak next to the main Bragg reflections stems from a contamination of the primary beam by the Cu $K\alpha_2$ line. During the data analysis both peaks have been refined by Gaussians with a Lorenzian background. The broad peaks close to $q_z\approx 4.75\,\text{Å}^{-1}$ are due to the $CoSi_2$ layers. Oscillations of the CTR for larger q_z values are caused by the finite thickness of the crystalline $CoSi_2$ layer and yield the Laue interference function. From a fit of the data with a

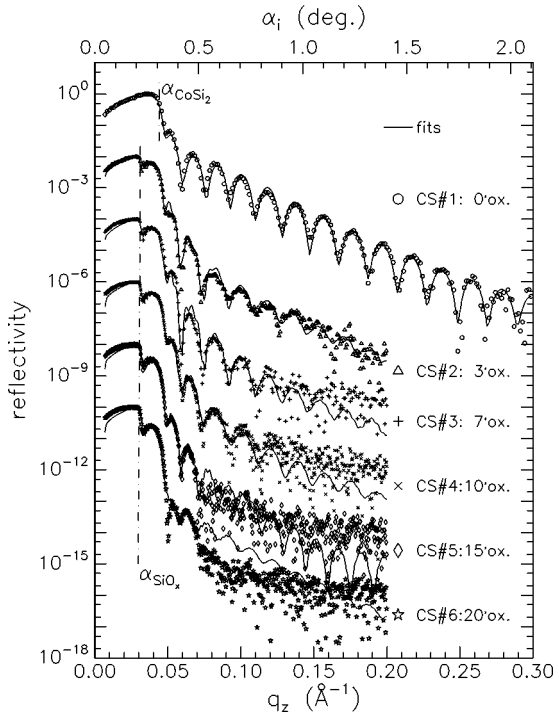

FIG. 3. True specular reflectivities (open circles) and fits (solid lines) for the nonoxidized sample CS#1 and the oxidized samples CS#2–CS#6. The critical angles of $CoSi_2$ and SiO_2 are marked by dashed–dotted lines. All curves are vertically shifted for clarity.

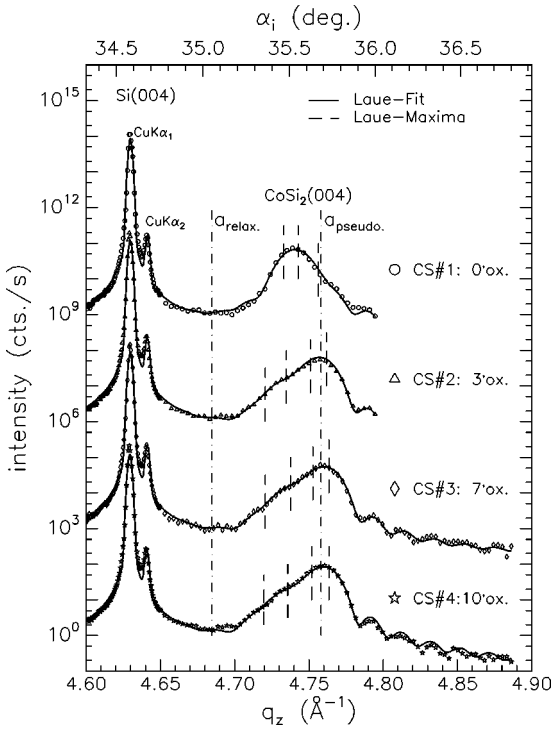

FIG. 4. CTR measurements (symbols) and fits with Laue interference functions (lines) for samples CS#1–CS#4. The dashed vertical lines correspond to the center of the Laue functions used for the calculations.

layer model, assuming a particular lattice constant distribution, the crystalline quality of the $CoSi_2$ layers may be obtained.

IV. RESULTS AND DISCUSSION

The following conclusions may be drawn from the true specular reflectivities shown in Fig. 3. In the case of perfect layers without interface roughnesses the x-ray reflectivity of a thin $CoSi_2$ layer underneath a thick SiO_2 layer is expected to yield two different well separated oscillations. However, interface roughnesses may modify the picture considerably. The reflectivities of Fig. 3 display only one distinct modulation. This modulation is most pronounced for the first reflectivity curve that corresponds to the nonoxidized sample. From the oscillation period a thickness of $d_{CoSi_2}=313$ Å of the $CoSi_2$ films is obtained. This is in good agreement with the value of 300 Å, which was determined by Rutherford backscattering spectroscopy.

The other fits suffer from the limited number of data points that are present after the subtraction of the diffuse scattering data. The $CoSi_2$ oscillations are still pronounced for all samples, while the SiO_2 layer is hardly visible. This is a clear indication of rough interfaces of the grown oxide layers. Since the true specular reflectivity drops more quickly for the samples with the larger oxidation times, the respective interfaces are less perfect. However, the information about the SiO_2 film thicknesses can be extracted more precisely from the dip in the intensity after the critical angle α_{c,SiO_2} corresponding to the oxide layer. Since $CoSi_2$ is the denser material ($\delta_{CoSi_2}>\delta_{SiO_2}$) the critical angle is larger and hence the reflected intensity increases even for $\alpha_i>\alpha_{c,SiO_2}$. Here the x rays can penetrate through the SiO_2 layer but they are still totally reflected by the $CoSi_2$ layer underneath. Since the reflected intensity is affected by absorption within the SiO_2 cap layer, one is nevertheless sensitive to the oxide layer thickness and interface morphologies. The information is contained in the drop of the reflectivity in the region $\alpha_{c,SiO_2}<\alpha_i<\alpha_{c,CoSi_2}$. The determination of the SiO_x film thicknesses and roughnesses from the drop after α_{c,SiO_2} is less accurate compared to a fit to reflectivity oscillations. Furthermore, the fits presented in Fig. 3 are far from being perfect for the samples with larger oxidation times. Therefore, the error bars are quite large.

All fit results are summarized in Table II and the respective dispersion (i.e., vertical electron density) profiles are displayed in Figs. 5 and 6. Here z is the coordinate perpendicular to the surface. The $CoSi_2$ layers can be seen clearly. The vertical dashed lines indicate the respective SiO_2/air interfaces. The density profiles reveal that the interfaces become rougher with increasing oxidation time. Particularly, the magnification of the density profiles of the $CoSi_2$ layers (see Fig. 6) shows that the quality of the buried films is strongly reduced by the oxidation process. This was also suggested by the diffusely scattered intensity as discussed before and can be seen in Fig. 3 where the true specular reflectivities are depicted.

Since the interfaces are very rough the so-called effective density model was used to explain the data. Within this model the density profiles are parametrized by layers with given probability functions. For a layer system with small roughnesses and thick layers, this leads to well separated

TABLE II. Parameters obtained from the fits of the true specular reflectivities for samples CS#1–CS#6. $f_\delta=(\delta-\delta_{\text{theo.}})/\delta_{\text{theo.}}$ is the dispersion (i.e., density) difference between the fit values δ and the theoretical value for $CoSi_2$ single crystals. Error bars are given in the second subcolumn for each quantity. The rms roughness of the interfaces is denoted by σ and the layer thicknesses by d. Transition layers between the SiO_2 layers and the $CoSi_2$ films and the $CoSi_2$ and the Si substrates have to be introduced to obtain good fits.

Sample	Layers	f_δ (%)	δ (10^{-6})	$\Delta\delta$ (10^{-6})	σ (Å)	$\Delta\sigma$ (Å)	d (Å)	Δd (Å)
CS#1	SiO_2	0	6.8	−5, +2	19.2	+20, −5	60.4	±10
	trans, layer	—	4.9	±2	33.7	±20	4.9	±10
	$CoSi_2$	−2.1	14.3	±1	8.6	±2	313.4	±2
	Si	—	7.6	—	9.9	±1	∞	—
CS#2	SiO_2	2.9	7.0	±1	43.2	+20, −5	692.4	±30
	trans. layer	—	10.1	±1	25.5	±5	8.2	+10, −8
	$CoSi_2$	0	14.6	±2	42.0	±5	361.0	±5
	trans. layer	—	9.0	±1	31.4	±5	8.6	±5
	Si	—	7.6	—	15.0	±2	∞	—
CS#3	SiO_2	5.15	7.1	±1	43.2	+20, −10	1058.6	±30
	trans. layer	—	10.0	±1	27.4	±5	13.8	±5
	$CoSi_2$	0.68	14.7	±2	52.8	±5	358.5	±5
	trans. layer	—	10.1	±1	32.7	±5	2.4	±5
	Si	—	7.6	—	15.0	±2	∞	—
CS#4	SiO_2	5.15	7.1	±1	43.2	+20, −10	1390.9	±40
	trans. layer	—	10.5	±1	27.0	±5	8.8	+10, −3
	$CoSi_2$	0.68	14.7	±2	49.4	±5	333.0	±5
	trans. layer	—	10.0	±1	41.0	±5	4.5	±5
	Si	—	7.6	—	15.8	±2	∞	—
CS#5	SiO_2	5.89	7.2	±1	43.2	±10	1792.3	>40
	trans. layer	—	8.9	±1	43.3	±5	7.6	±10
	$CoSi_2$	2.74	15.0	±2	69.1	±5	335.9	±10
	trans. layer	—	10.3	±1	39.9	±5	32.5	±10
	Si	—	7.6	—	13.4	±2	∞	—
CS#6	SiO_2	7.35	7.3	±1	40.0	+10, −5	1945.8	>40
	trans. layer	—	8.6	±1	90.8	±5	36.4	±10
	$CoSi_2$	2.74	15.0	±2	54.5	±5	320.7	±15
	trans. layer	—	10.2	±1	54.0	±5	60.1	±10
	Si	—	7.6	—	10.5	±5	∞	—

interfaces and the Parratt formalism to calculate the reflectivity may be applied. Arbitrary continuous density profiles are modeled by introducing very thin and rough transition layers. To calculate the reflectivity with the Parratt formalism the profile needs then to be sliced into very small sublayers. In this case, one has to check the meaning of the roughness and the layer thickness of the transition layers very carefully, because the roughness may exceed the thickness (even negative thicknesses would be allowed). These values should be treated as parameters which model the actual density profile and not as properties of the layers (for details see Ref. 34 and references therein).

The nature of the oxide growth process may also be extracted quantitatively from our data. An increase of the thickness d_{SiO_2} of the SiO_2 layers with increasing oxidation time t can be seen. This increase may be explained with a linear-quadratic growth model yielding the following equation for the time dependence of d_{SiO_2}:[11]

$$[d_{SiO_2}(t)]^2+Ad_{SiO_2}(t)=B(t+\tau), \tag{1}$$

with the oxidation time t, constants A and B which are connected with the respective growth parameters (diffusion constants, concentrations etc.), and $\tau=(d_0^2+Ad_0)/B$, where d_0 is an oxide layer that is present before the wet oxidation process starts.[35–40] For large times t the linear term in Eq. (1) may be neglected and one obtains a purely quadratic growth law

$$d_{SiO_2}(t)=\sqrt{B(t+\tau)}, \tag{2}$$

where B is essentially proportional to the diffusion constant of the oxygen transport through the oxide layer. Since the oxygen diffusion is the slowest process in the formation of the oxide layer, the growth of the oxide layer of our samples is diffusion limited. Figure 7 shows the thicknesses of the SiO_2 layers obtained from the fits of the true specular reflectivity data versus the oxidation time t. A fit with Eq. (2) is given by the solid line in Fig. 7. The square-root increase ($\tau\approx0$) of the film thickness can be seen clearly, suggesting that the growth of the oxide layers is indeed diffusion limited.

While the above considerations only yield information about the mesoscopic properties of the samples, atomic information has to be extracted from scattering around Bragg

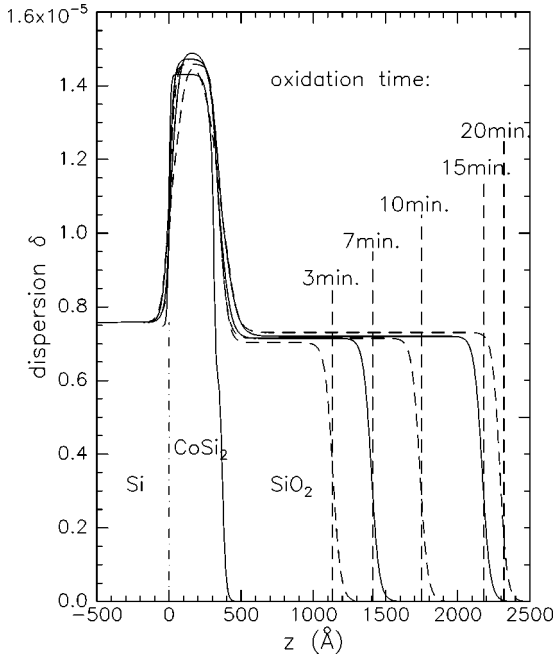

FIG. 5. Dispersion (electron density) profiles of the nonoxidized and oxidized samples as obtained from the fits of the true specular reflectivities. The layered systems are clearly visible. The dashed lines indicate the thickness of the SiO_2 layers after the respective oxidation times.

reflections.[25] Figure 4 shows the data and the fits for the nonoxidized sample CS#1 and for samples CS#2, CS#3, and CS#4.

First of all the maximum of the broad $CoSi_2$ (004) reflection of the nonoxidized sample CS#1 is located at $q_z = 4.74\,\text{Å}^{-1}$, which is between the value for a completely relaxed structure and that of a pseudomorphically grown $CoSi_2$ layer, whereas the q_z value of the $CoSi_2$ peaks for the oxidized samples $q_z = 4.76\,\text{Å}^{-1}$ is remarkably larger. The position corresponds to the compressed vertical lattice constant for a completely pseudomorphic $CoSi_2$ layer on

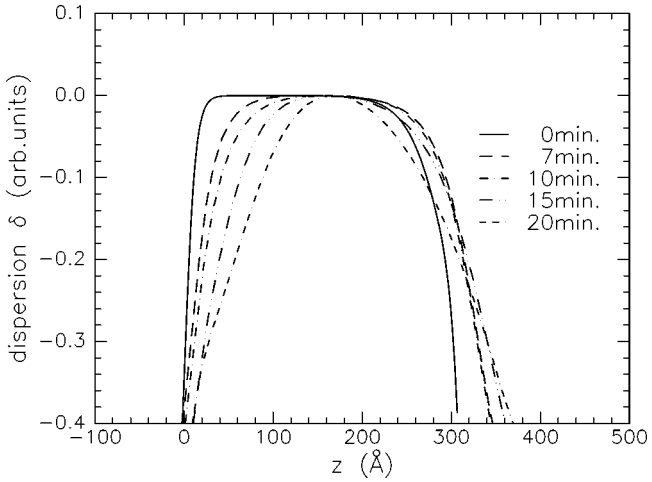

FIG. 6. Magnification of the $CoSi_2$ part of the dispersion (electron density) profiles (see Fig. 6). For clarity all profiles are normalized to the respective maximum values. The interfaces of the $CoSi_2$ layer are less sharp with increasing oxidation time.

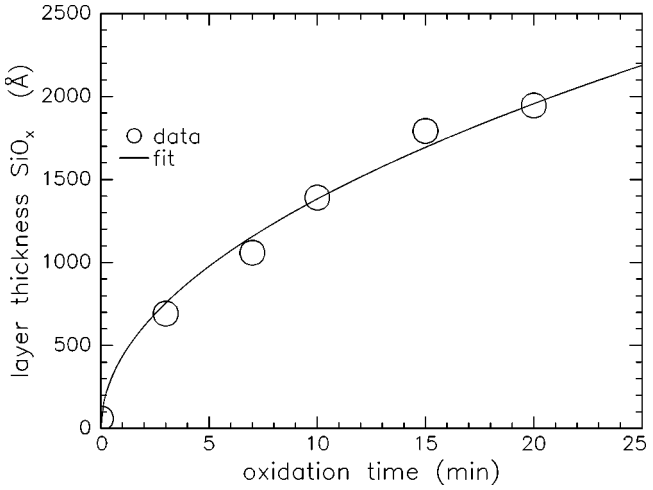

FIG. 7. Obtained SiO_2 layer thicknesses vs oxidation time (open circles). The data suggest a quadratic growth model (solid line fit).

Si(001).[3] This shows that the oxidation process increases the strain in the $CoSi_2$ layer.

The broad $CoSi_2$ Bragg peaks were refined more quantitatively with overlapping Laue interference functions, whose maxima are at the location of the vertical dashed lines in Fig. 4. For the nonoxidized sample three Laue functions are necessary to explain the data points. This shows that even for sample CS#1 a certain degree of strain is present in the $CoSi_2$ layer. The strain increases by the subsequent oxidation because the data for the oxidized samples have to be explained by assuming at least four Laue functions. Furthermore, this is in agreement with our recent results for buried $CoSi_2$ layers.[3] The positions of the maxima yield the mean lattice constants of the $CoSi_2$ layers. This may suggest that the layers did not grow homogeneously over the sample area. Table III summarizes the results of the Laue fits.

Fitting the $CoSi_2$ Bragg peaks with different Laue functions means that the samples consist of laterally separated regions with different lattice constants and therefore different amounts of strain. A TEM micrograph of sample CS#4 (Fig. 8) revealed that the sample locally possesses smooth interfaces with a spatial extend of about 3000 Å but with varying layer thicknesses on larger length scales. This explains both the large rms roughness and the broad strain distribution. The large rms roughness stems from the lateral averaging over a surface area which is 100 times larger than the size of the smooth interface regions, and therefore represents prima-

TABLE III. Results of the Laue function fits of the CTRs for samples CS#1–CS#4. The lattice constant of totally relaxed $CoSi_2$ is $a_{\text{rel.}} = 5.365$ Å and for a pseudomorphic film on Si(001) the vertical lattice parameter is $a_{\text{pse.}} = 5.282$ Å.

Sample	CS#1	CS#2	CS#3	CS#4
$CoSi_2$ thicknesses (Å)	310	326	317	320
Lattice constants	5.284	5.278	5.276	5.276
of the Laue	5.299	5.290	5.288	5.289
functions	5.310	5.308	5.305	5.307
(Å)	—	5.324	5.324	5.325

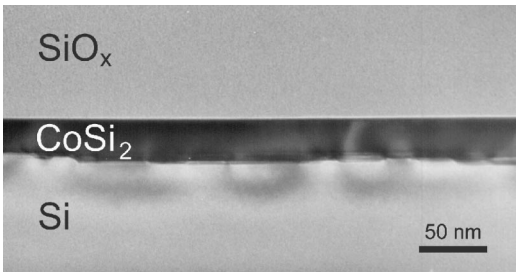

FIG. 8. ⟨110⟩ TEM cross section image of sample CS#4.

rily the thickness variation of the $CoSi_2$ layer. Depending on the local thickness, the strain in the $CoSi_2$ and the adjacent Si substrate varies as can be seen in the TEM micrograph (Fig. 8). This leads to the observed broad lattice parameter distribution of the oxidized samples.

V. SUMMARY AND OUTLOOK

We have investigated buried $CoSi_2$ layer systems by x-ray specular reflectivity and crystal truncation rod scattering. The samples were prepared by MBA and a subsequent wet oxidation process.

It is shown that the formation of the oxide layers on top of the $CoSi_2$ films is a diffusion limited process. This was identified by a quadratic growth law for the oxide formation. The nonoxidized sample shows well defined oscillations of the true specular reflectivity corresponding to a $CoSi_2$ layer with small interface roughness. The subsequent oxidation process leads to a drastic increase of the interfacial roughnesses: The longer the oxidation process takes place, i.e., the thicker the cap oxide layer is, the rougher the interfaces are. The density profiles reveal further that the increase of the roughness can be detected at both sides of the $CoSi_2$ layer. The crystalline quality of the layer systems was investigated by CTR measurements around the (004) Si and $CoSi_2$ Bragg reflections. All measurements show asymmetric $CoSi_2$ peaks that can be explained by a lattice constant variation over the sample surface. Nevertheless, the oxidation leads to a strong pseudomorphic structure.

Further investigations of samples that have been prepared under different growth conditions may yield information about preparation parameters, which leads to samples with better interface quality. These samples may be of considerable interest for future applications in microelectronic devices.

ACKNOWLEDGMENT

This work was supported by the Volkswagenstiftung under Project No. I/71128.

[1] R. Stadler, C. Schwarz, H. Sirringhaus, and H. von Känel, Surf. Sci. **271**, 355 (1992).
[2] J. Stettner, L. Schwalowsky, M. Tolan, O. H. Seeck, W. Press, C. Schwartz, and H. v. Känel, Phys. Rev. B **53**, 1398 (1996).
[3] U. Zimmermann, J.-P. Schlomka, M. Tolan, J. Stettner, W. Press, M. Hacke, and S. Mantl, J. Appl. Phys. **83**, 5823 (1998).
[4] S. Mantl; Mater. Sci. Rep. **8**, 1 (1992).
[5] D. Bahr, W. Press, R. Jebasinski, and S. Mantl, Phys. Rev. B **47**, 4385 (1993).
[6] M. Müller, D. Bahr, W. Press, R. Jebasinski, and S. Mantl, J. Appl. Phys. **74**, 1590 (1993).
[7] S. Mantl and H. L. Bay, Appl. Phys. Lett. **61**, 267 (1992).
[8] S. Mantl, J. Phys. D **31**, 1 (1998).
[9] S. Mantl, M. Dolle, St. Mesters, P. F. P. Fichtner, and H. L. Bay, Appl. Phys. Lett. **67**, 3459 (1995).
[10] F. Klinkhammer *et al.*, Microelectron. Eng. **37/38**, 515 (1997).
[11] F. Klinkhammer, PhD thesis, RWTH, Aachen 1998.
[12] Q. T. Zhao, F. Klinkhammer, M. Dolle, L. Kappius, and S. Mantl, Appl. Phys. Lett. **74**, 454 (1999).
[13] S. Mantl, Mater. Res. Soc. Symp. Proc. **1**, 514 (1998).
[14] S. K. Sinha, E. B. Sirota, S. Garoff, and H. B. Stanley, Phys. Rev. B **38**, 2297 (1988).
[15] R. Pynn, Phys. Rev. B **45**, 602 (1992).
[16] D. K. G. de Boer, Phys. Rev. B **49**, 5817 (1994).
[17] D. K. G. de Boer, Phys. Rev. B **51**, 5297 (1995).
[18] V. Holý, J. Kuběna, I. Ohlídal, K. Lischka, and W. Plotz, Phys. Rev. B **47**, 15896 (1993).
[19] V. Holý and T. Baumbach, Phys. Rev. B **49**, 10668 (1994).
[20] S. Dietrich and A. Haase, Phys. Rep. **260**, 1 (1995).
[21] T. Salditt, T. H. Metzger, and J. Peisl, Phys. Rev. Lett. **73**, 2228 (1994).
[22] J.-P. Schlomka, M. Tolan, L. Schwalowsky, O. H. Seeck, J. Stettner, and W. Press, Phys. Rev. B **51**, 2311 (1995).
[23] S. R. Andrews and R. A. Cowley, J. Phys. C **18**, 6427 (1985).
[24] I. K. Robinson, Phys. Rev. B **33**, 3830 (1986).
[25] V. Holý, U. Pietsch, and T. Baumbach, *X-Ray Scattering from Thin Films (High Resolution X-Ray Scattering from Crystalline Thin Films)*, Springer Tracts in Modern Physics, Vol. 149 (Springer, Berlin, 1999).
[26] R. W. James, *The Optical Principles of the Diffraction of X-Rays* (Ox Bow Press, Woodbridge, 1962).
[27] L. G. Parratt, Phys. Rev. **95**, 359 (1954).
[28] H. Dosch, *Critical Phenomena at Surfaces and Interfaces (Evanescent X-Ray and Neutron Scattering)*, Springer Tracts in Modern Physics, Vol. 126 (Springer, Berlin, 1992).
[29] F. Abelès, Ann. Phys. (Paris) **5**, 596 (1950).
[30] J. Lekner, *Theory of Reflection* (Nijhoff, Dordrecht, 1987).
[31] M. Born and E. Wolf, *Principles of Optics* (Pergamon, Oxford, 1993).
[32] Theoretically the reflectivity has to be unity for $q_z < q_{z,c}$ and is only slightly damped by absorption. For small incidence angles α_i most of the incoming radiation does not hit the sample and therefore an increasing of the reflectivity with increasing q_z rather than a horizontal plateau is observed. This purely geometrical correction is taken into account in the refinements and does not contain any information about the sample structure.
[33] Y. Yoneda, Phys. Rev. **131**, 2010 (1963).
[34] M. Tolan, *X-Ray Scattering from Soft-Matter Thin Films-Materials Science and Basic Research*, Springer Tracts in Modern Physics, Vol. 148 (Springer, Berlin, 1999).
[35] S. M. Sze, *VSLI Technology*, 2nd ed. (McGraw–Hill, New York, 1988).
[36] S. Wolf and R. N. Tauber, *Silicon Processing for the VLSI Era*, Vol. 1 (Lattice, Sunset Beach, CA, 1989).
[37] E. H. Nicollian and J. R. Brews, *MOS Physics and Technology* (Wiley, New York, 1982).
[38] E. A. Irene, *The Physics and Chemistry of the SiO_2 and the $Si-SiO_2$ Interface* (Plenum New York, 1988).
[39] B. E. Deal, *The Physics and Chemistry of the SiO_2 and the $Si-SiO_2$ Interface* (Plenum, New York, 1988).
[40] B. E. Deal and A. S. Grove, J. Appl. Phys. **36**, 3770 (1965).